SEMARAK ILMU PUBLISHING

Journal of Advanced Research in Fluid Mechanics and Thermal Sciences

Journal homepage:
https://semarakilmu.com.my/journals/index.php/fluid_mechanics_thermal_sciences/index
ISSN: 2289-7879

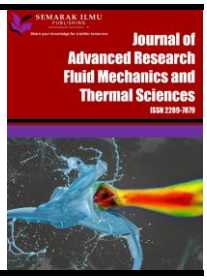

Extended Eddy-Viscosity Model to Rayleigh-Benard Convection in Cavity

Gunarjo Suryanto Budi[1,*], Sasa Kenjeres[2]

[1] Department of Physics Education, University of Palangka Raya, Palangka Raya, Central Kalimantan, Indonesia
[2] Department of Chemical Engineering, Faculty of Applied Sciences, Delft University of Technology, Van der Maasweg 9, 2629 HZ Delft, Netherlands

ARTICLE INFO

Article history:
Received 27 October 2023
Received in revised form 27 March 2024
Accepted 8 April 2024
Available online 30 April 2024

Keywords:
Turbulence; algebraic model; large eddy; Rayleigh-Benard convection

ABSTRACT

This paper presents a study of developing a numerical turbulent model in a cavity heated from below using eddy viscosity combined with elliptic relaxation approach. The model uses a set of differential equations that consist of kinetic energy, its dissipation, variance of temperature, velocity scale and elliptic relaxation parameter, which are solved using a finite-volume and Navier-Stokes solver. The unresolved stress tensors and heat flux vectors are modelled with an algebraic formula. The discretization method is carried out by CDS, or second-order differencing scheme, and LUDS, or second-order linear upwind scheme. The model is applied to the natural convection heated from below, known as Rayleigh-Benard convection, in a two-dimensional cavity with a height-to-length aspect ratio of 1:1.5, 1:4, and 1:8. The model has been validated using numerical data from DNS (direct numerical simulation) and experiments. The model produced similar results with both DNS and experiments. It was also shown that the model can visualize the main feature of turbulent convective flow in the enclosure for various aspect ratio.

1. Introduction

There has been an extensive study on natural convection in cavities for various geometry and a wide range of turbulence levels, namely by Gunarjo [1], Clifford and Kimber [2], Ji [3], and Saury *et al.,* [4]. The authors have applied the Boussinesq approximation as the mathematical basis in developing their models, in which all properties are assumed to be constant while density is treated as a variable of gravity that is linearly proportional to temperature. This leads to buoyancy-driven flow that generates turbulence around the cavity. The benchmark of such a study was the heat transfer of turbulent flow in the side-heated vertical rectangular cavities. There have also been many works dedicated to the study of heat transfer in buoyancy-driven flow in different orientations; instead of heated from the side, it is heated from below and cooled from above.

Natural convection buoyancy-driven flow heated from below has a lot of research attention as it has many engineering applications. Examples are the heating system inside buildings, heating of electronic compartments, heat exchanger systems, etc. Such real applications need to be studied in

* *Corresponding author.*
E-mail address: gunarjo.budi@chem.upr.ac.id

https://doi.org/10.37934/arfmts.116.2.102111

both an experimental and a numerical way, where turbulence models play an important role. In order to validate the turbulence model, it requires numerical data and experiments. However, the availability of Numerical data from the Direct Numerical Simulation DNS and experiment were limited. DNS data of such flow were provided by Demou and Grigoriadis [5] in the work of convective flow heated from below in water.

Modeling the heat and mass transfer of turbulent convective flow heated from below has been carried out by Kenjereš and Hanjalić [6] using transient analysis with the Reynold Averaged Navier-Stokes approach. The author demonstrated the performance of the model and compared it to DNS and the Large Eddy Simulation for a wide range of Rayleigh numbers. It is very obvious that the higher the Rayleigh number, the higher the turbulence level. When *Ra* is low, the model is similar to both the DNS and the experiment; however, it is quite different when *Ra* is high. Kenjereš and Hanjalić [6] noted that the large eddy simulation was over-predicted by almost 40% due to not accounting for the direct effect of buoyancy on the heat flux. In addition, the discrepancy of the large eddy simulation is also due to the presumption of a full alignment between components of the turbulent heat flux and mean temperature gradient. Improvement of the Large Eddy Simulation was demonstrated by Clifford and Kimber [7] in the study of Assessment on the model of RANS and LES for convective flow in a square cavity heated from the side, in which the model yielded nearly identical results from both DNS and experiment.

Numerical study of influences aspect ratio on heat transfer in two horizontal walls heated from below and cooled from above was carried out by van der Poel *et al.,* [8]. It was observed that the bigger the aspect ratio the less significant the influence. Similarly, investigation of the dependency of Nusselt number *Nu* and Reynold number *Re* on Rayleigh number *Ra* and aspect ratio. When the *Ra* is 10^6 and the aspect ratio is less than 1/3 four roll structure moving upwards across the center of cavity is obtained. However, dominant single roll structure is found when Ra is bigger than 10^7 and aspect ratio is small. The structure of the modelling the turbulent flow in enclosure heated from below and cooled from above for the transition to the ultimate regime, in which the boundary layer and the bulk are both turbulent was done by Zhu *et al.,* [9].

It is proposed that turbulent model should be mathematically simple, robust and can be applied in several cases. This study aims to simulate the convective flow in cavity for different aspect ratios heated from below using eddy-viscosity with elliptic relaxation and algebraic approaches. The model consists of five differential equations namely turbulent kinetic energy, dissipation, temperature variance, scalar *rms* turbulent fluctuation and elliptic relaxation parameter Kenjereš *et al.,* [10]. The model is evaluated with available direct numerical simulation and experiment.

2. Methodology

2.1 Numerical Method

The computation of the turbulence flow heated from below was carried out using a numerical method that includes several steps, namely grid generation, discretization, calculation, data analysis, and visualization. The computer code was developed and employed by Kenjereš *et al.,* [10], Kenjereš [11], and Gunarjo [1], and its performance is very good, robust, insensitive of grid resolution and applicable for many turbulent flows. The grids were generated in non-orthogonal geometries using the collocated arrangement of Ferziger and Perić [12]. The differential equations containing kinetic energy, dissipation, variance of temperature, scalar of *rms* turbulent fluctuation and elliptic relaxation parameter were solved numerically by using finite-volume and Navier-Stokes solvers. The diffusive terms of the transport were discretized by using the second-order central differencing scheme CDS, while the convective terms of the transport were discretized by using the second-order

linear upwind scheme LUDS. Discretization of the coupling between pressure fields and velocity was done using the SIMPLE (Semi Implicit Method for Pressure-Linked Equations) algorithm of Patankar [13]. It is important to note that to reach stability and a convergent solution for the fields, we applied each part of a different under relaxation factor and maintained the false time step at the same number. A convergence solution was reached when the maximum absolute values varied less than 10^{-6} between two successive iterations.

Figure 1 illustrates the grids of the calculation for (a) a height-to-length aspect ratio of 1:1.5, (b) an aspect ratio of 1:4, and (c) an aspect ratio of 1:8. The meshes in the near wall are very fine to accurately capture the fields where heat and mass transfer of turbulence flow are intensive. Contrary to this, coarse mesh was applied in the region far from the wall, especially in the central area where heat and mass transfer of turbulence flow are stagnant.

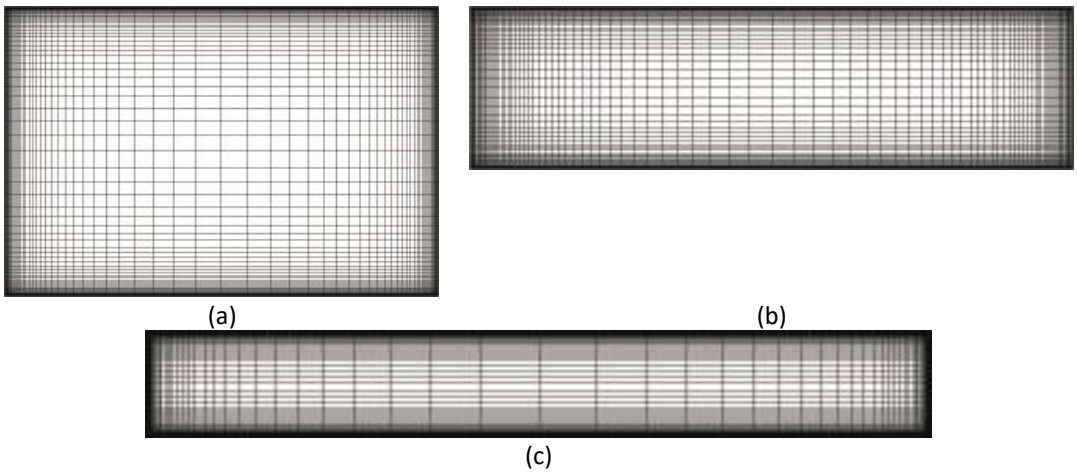

Fig. 1. The collocated grid of two-dimensional cavity for the height to length ratio of (a) *H*/*L* = 1:1.5, (b) *H*/*L* = 1:4 and (c) *H*/*L* = 1:8

2.2 Turbulent Model

Turbulent flow and heat mass transfer are fully defined in the conservation equation for mass, momentum, and energy for instantaneous motion. Introducing Reynolds averaging and Boussinesq approximation, the equations can be written as

$$\frac{\partial \rho}{\partial t} + \frac{\partial \rho U_j}{\partial x_j} = 0 \tag{1}$$

$$\frac{\partial \rho U_i}{\partial t} + U_j \frac{\partial \rho U_i}{\partial x_j} = -\frac{\partial P}{\partial x_i} + \frac{\partial}{\partial x_j}\left[\mu\left(\frac{\partial U_i}{\partial x_j} + \frac{\partial U_j}{\partial x_i}\right) - \rho\overline{u_i u_j}\right] + \rho\beta g_i\,(T - T_{ref}) \tag{2}$$

$$\frac{\partial \rho T}{\partial t} + U_j \frac{\partial \rho T}{\partial x_j} = \frac{\partial}{\partial x_i}\left(\frac{\mu}{P_r}\frac{\partial T}{\partial x_i} - \rho\,\overline{\theta u_i}\right) \tag{3}$$

The transport equation of turbulent kinetic energy k, the dissipation ε and temperature variance $\overline{\theta^2}$ read

$$\frac{Dk}{Dt} = -\overline{u_i u_k}\frac{\partial U_i}{\partial x_k} + \rho\beta g_i \overline{\theta u_i} - \varepsilon + \frac{\partial}{\partial x_k}\left[\left(\nu + \frac{\nu_t}{\sigma_k}\right)\frac{\partial k}{\partial x_j}\right] \tag{4}$$

$$\frac{D\varepsilon}{Dt} = \frac{C_1(Pi+G) - C_2\varepsilon}{\tau} + \frac{\partial}{\partial x_j}\left[\left(\nu + \frac{\nu_t}{\sigma_\varepsilon}\right)\frac{\partial \varepsilon}{\partial x_j}\right] \tag{5}$$

$$\frac{D\overline{\theta^2}}{Dt} = -2\overline{\theta u_j}\frac{\partial T}{\partial x_j} - 2\varepsilon_\theta + \frac{\partial}{\partial x_j}\left[\left(\nu + \frac{\nu_t}{\sigma_{\theta^2}}\right)\frac{\partial \overline{\theta^2}}{\partial x_j}\right] \tag{6}$$

Averaging the equation using RANS introduces the second-moment Reynolds stress tensors $\overline{u_\iota u_J}$ and the turbulent heat flux vector $\overline{\theta u_\iota}$. They need to be modelled by the simplest approach based on the eddy viscosity/diffusivity concept, where the Reynolds stress tensors and heat flux vectors are expressed in terms of averaged velocity and temperature gradient, respectively, i.e.,

$$\overline{u_\iota u_J} = \frac{2}{3}\mathrm{k}\delta_{ij} - \upsilon_t\left(\frac{\partial U_i}{\partial x_j} + \frac{\partial U_j}{\partial x_i}\right) \tag{7}$$

$$\overline{\theta u_\iota} = \frac{\upsilon_t}{\sigma_t}\frac{\partial T}{\partial x_i} \tag{8}$$

where σ_t denotes the turbulent Prandtl number.

For the eddy viscosity model, usually a dumping function is formulated in terms of the *Ra* number and added to the equation of velocity scale υt by Jones and Launder [14], and this leads to the requirement for solving the equation of kinetic energy *k*. The most common approach is to use the length scale *L*, especially at high Reynolds numbers. The length scale can be defined using pure similarity arguments and dimensional analysis in terms of kinetic energy and the dissipation rate and this leads to $L\ \alpha\ k^{3/2}/\varepsilon$. In this study, the eddy viscosity is extended into an algebraic equation to account for the strong effect of buoyancy, which is defined as

$$\overline{u_i u_j} = \frac{2}{3}k\delta_{ij} - C_\mu\tau\overline{v^2}\left(\frac{\partial U_i}{\partial x_j} + \frac{\partial U_j}{\partial x_i}\right) + C_\theta\tau\beta g_j\overline{\theta u_i} \tag{9}$$

$$\overline{\theta u_i} = -C_\theta\tau\left(\varsigma\overline{u_i u_j}\frac{\partial T}{\partial x_j} + \xi\overline{\theta u_j}\frac{\partial U_i}{\partial x_j} + \beta g_i\overline{\theta^2}\right) \tag{10}$$

The coefficients in the equations are given: $C_1 = 1.4, C_2 = 0.6, C_\mu = 0.22, C_L = 0.2, C_T = 6, C_\theta = 0.5, C\eta = 50$. The proposed extended eddy-viscosity turbulent model consists of five equations, namely Eq. (4), Eq. (5), Eq. (6), differential equations of scalar *rms* turbulent fluctuation $\overline{v^2}$ and elliptic relaxation parameter *f* and the algebraic expression of Eq. (9) and Eq. (10) as derived by Kenjereš [11]. It can be seen from the equations that they are not only simple but also robust and accurate.

3. Results

3.1 Validation of the Model and Result

In this section, numerical simulation results in horizontal channel at *Ra* = 10^9 are presented in Figure 2, Figure 3, Figure 4, Figure 5, Figure 6 and are validated by data from direct numerical simulation of Wörner [15]. Figure 2 shows the profiles of the dissipation rate of temperature variance

and heat flux. It was clear that the present model fitted the data quite well, especially in the near wall area. This might be due to the inclusion of buoyancy into the Reynolds stress tensors and heat flux vectors, which were able to present the main fields of turbulence in the buoyancy-driven flow. However, disparity is observed for the dissipation rate of heat flux in the middle of cavity, in which the model is under prediction.

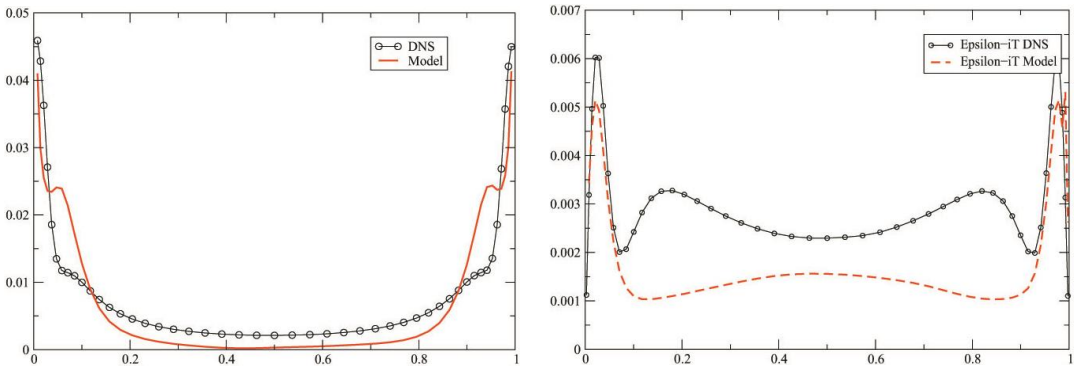

(a) (b)

Fig. 2. Plots of dissipation rate of (a) temperature variance, (b) heat flux of Rayleigh-Benard convection of DNS, simulation with the present model at Ra = 6.3 x 10^5

Figure 3 shows the plot of the present model and DNS for the Reynolds stress $\overline{uu}, \overline{vv}, \text{and } \overline{ww}$ components. It can be seen that the present model reproduced well the shape of DNS. The stress $\overline{ww}$ captured the peak very well, however the model of $\overline{uu}$ and $\overline{vv}$ is slightly under predicted. The profile of heat flux of the present model is plotted with model of Dol *et al.,* [16], the basic model and the DNS in Figure 4. All models produced peaks in the near conducting walls, while in the middle of cavity is wavy shaped. Similar prediction is observed between the present model and Dol *et al.,* [16] but it is observed that the present model calculated heat flux better in the middle cavity.

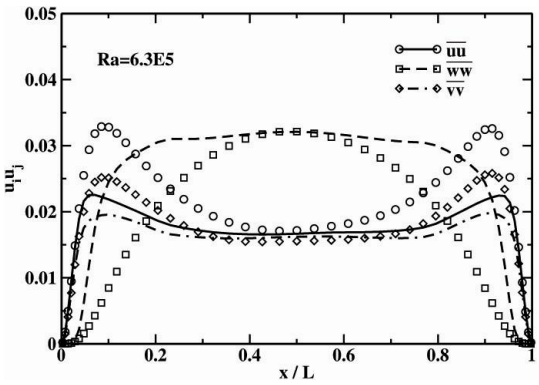

Fig. 3. Plots of stress uu, vv, ww pada Rayleigh-Benard convection Ra = 6.3 x 10^5 DNS and the present model

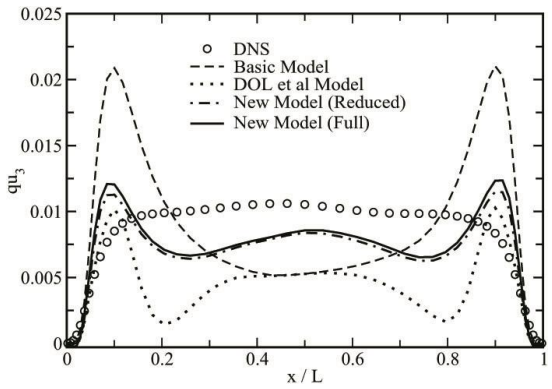

Fig. 4. Plots of heat flux of Rayleigh-Benard convection DNS, basic model, Dol *et al.,* [16] model and the present model

Figure 5 shows the plots of the thermal-to-mechanical time scale ratio of Direct Numerical Simulation DNS for Rayleigh-Benard convection in a horizontal channel heated from below by Wörner [15]. In order to improve the performance of the model, we propose an expression for the time-scale ratio *R* by

$$R = \max\left[\left(\frac{A_{2\theta}^{\frac{1}{2}}}{1+A_{2\theta}}\right), 0.6A\right] \tag{11}$$

where $A_{2\theta}$ denotes scalar flux invariant.

The model is also validated by the calculation by Craft [17], who developed a model for the time scale ratio as $R = 1.5\ (1 + A_{2\theta})^{-1}$. It is obvious that, overall, the present model yields nearly identical results to Craft [17], but an improvement is observed in the near-wall region, where the present model of Eq. (11) captured the thermal to mechanical time scale aspect ratio well. It is interesting to note that the present model was able to follow the main feature of DNS in both near-wall regions and in the remaining area of the cavity; however, a reasonable disparity is found in the central zone, where the peak of DNS reached 1 while the model is around 0.6.

The computed temperature profile for $Ra = 2 \times 10^9$ are plotted against the numerical result of Kenjereš *et al.,* [10] and measured temperature for $Ra = 10^6$ of Chu and Goldstein [18] in Figure 6. The proposed model fitted very well the model of Kenjereš [11] for calculation at the same Rayleigh number and the model of $Ra = 10^6$ predicted well the experiment.

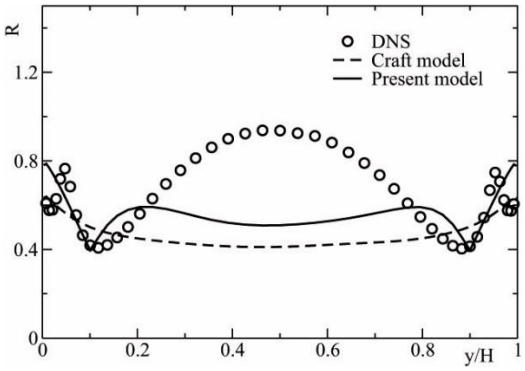

Fig. 5. Plots of the thermal to mechanical time scale ratio of Rayleigh-Benard convection of DNS, simulation by Craft [17] and the present model

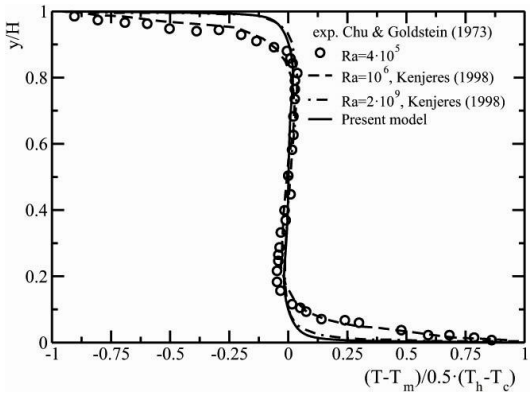

Fig. 6. The profile of temperature at isothermal wall of Rayleigh-Benard Convection with experiment by Chu and Goldstein [18]

The numerical simulation of convective flow in the cavity of various aspect ratios with first grid distance from the wall $y_n = 10^{-3}$, grid expansion factor 1.1, Rayleigh number $Ra = 2 \times 10^9$, Prand number $Pr = 0.71$ is presented in this section. The grid for the simulation is 82 x 82 of non-uniform collocated one with fine spacing near the horizontal walls to capture the steep gradient in the thin boundary layers. The insight of the main feature of convective flow in the cavity heated from below is presented in Figure 7, Figure 8, and Figure 9. The velocity vectors in the cavity are given for various height-to-length ratios (H/L), namely H/L = 1:1.5, H/L = 1:4, and H/L = 1:8 in Figure 7(a), Figure 7(b), and Figure 7(c). The stream lines and distribution of local Nusselt numbers are given in Figure 8(a), Figure 8(b), Figure 8(c), and in Figure 9(a), Figure 9(b), and Figure 9(c), respectively.

It can be seen from Figure 7 that generally intensive flow occurs only in the near wall, while in the middle of the cavity it is very quiet, which indicates that intensive heat transfer occurs in the near wall region only while in the middle it is stagnant. As can be seen from Figure 7(a), the flow in the central zone of the cavity with H/L = 1:1.5 is very rare, even almost empty, and this indicates characteristics of a laminar flow. It is observed from the figure that there is a big circulating flow in clockwise direction with a relatively narrow layer along the conducting walls. This suggests that the majority of turbulence is located in the regions and is reduced to a very small magnitude in the middle

of the cavity. The velocity vector plot with *H*/*L* = 1:4 in Figure 7(b) introduces a very interesting feature. There were two big circulating flows of symmetrical shapes in the right and left regions, one clockwise and the other counter clockwise. In addition, the turbulence regime was observed and confined to the near-conducting walls. Quite complex and more circulating flow in the cavity with *H*/*L* = 1:8 is plotted in Figure 7(c). Three distinctive patterns were observed: (1) two circulating flows located at the end of non-conducting walls; (2) two circulating flows that created irregular features tilted in the direction of the upper corners of the cavity; and (3) the stagnation region of the laminar regime with a V-shaped situated in the central cavity. It is important to note that the turbulence regime was found in the quarter part of the left and right conducting walls, while the most intensive heat and mass transfer was found in the bottom corners of the cavity.

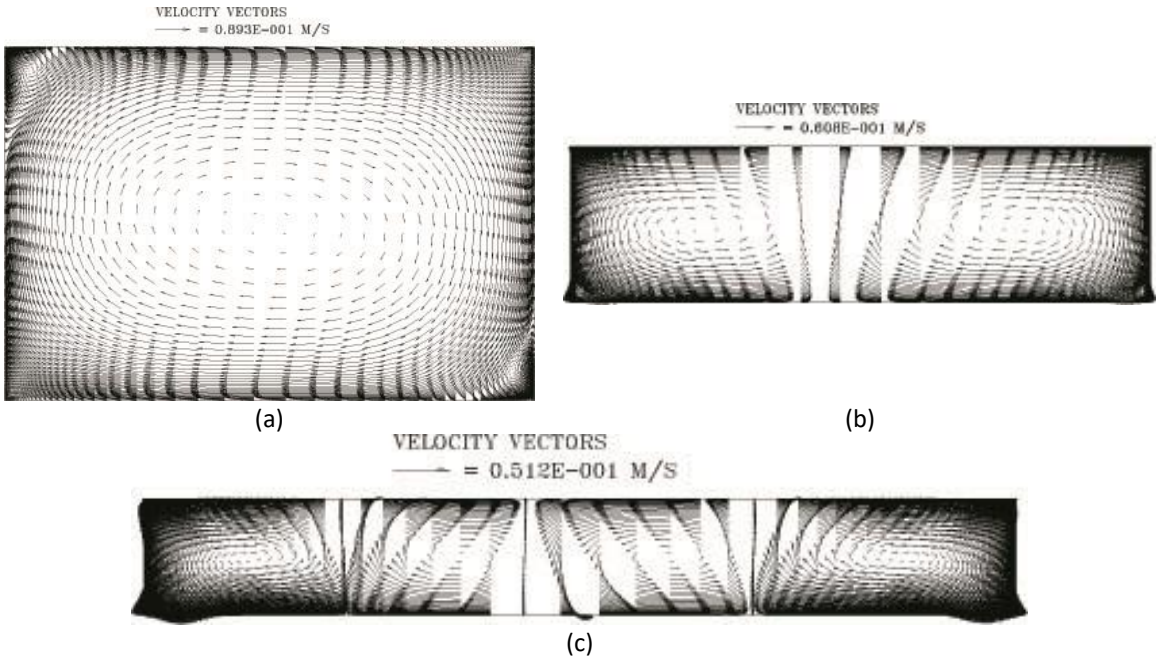

Fig. 7. The plots of velocity vectors in the cavity are given for various height to length ratio (*H/L*), namely (a) *H*/*L* = 1:1.5, (b) *H*/*L* = 1:4 and (c) *H*/*L* = 1:8

Figure 8(a), Figure 8(b), and Figure 8(c) show the flow stream lines of the simulation for the height-to-length aspect ratio *H*/*L* = 1: 1.5, 1: 4, and 1: 8, respectively. Solid lines indicate counter clockwise flow, while dash lines indicate clockwise flow. One big rotating flow is observed in the cavity with a ratio of *H*/*L* = 1:1.5, while two symmetrical rotating flows are found in *H*/*L* = 1:4, and four symmetrical circulating flows are seen in *H*/*L* = 1:8. It can be mentioned that the number of circulations is half of the ratio; for example, if the height-to-length ratio is 1:16, the number of circulations is 8, etc.

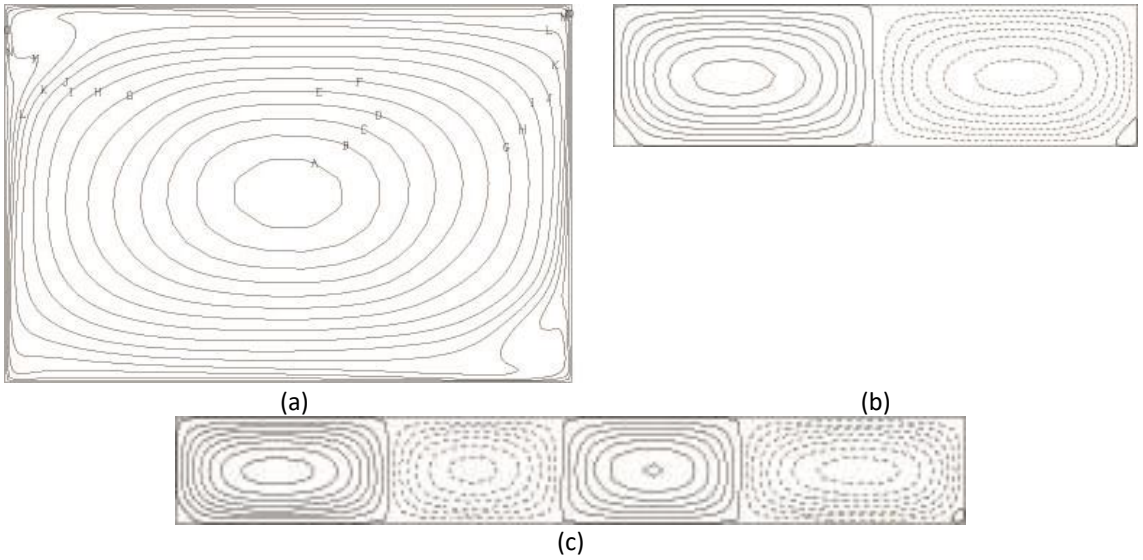

(a) (b)

(c)

Fig. 8. The stream lines in the cavity for various height-to-length ratios (a) *H*/*L* = 1:1.5, (b) *H*/*L* = 1:4, and (c) *H*/*L* = 1:8

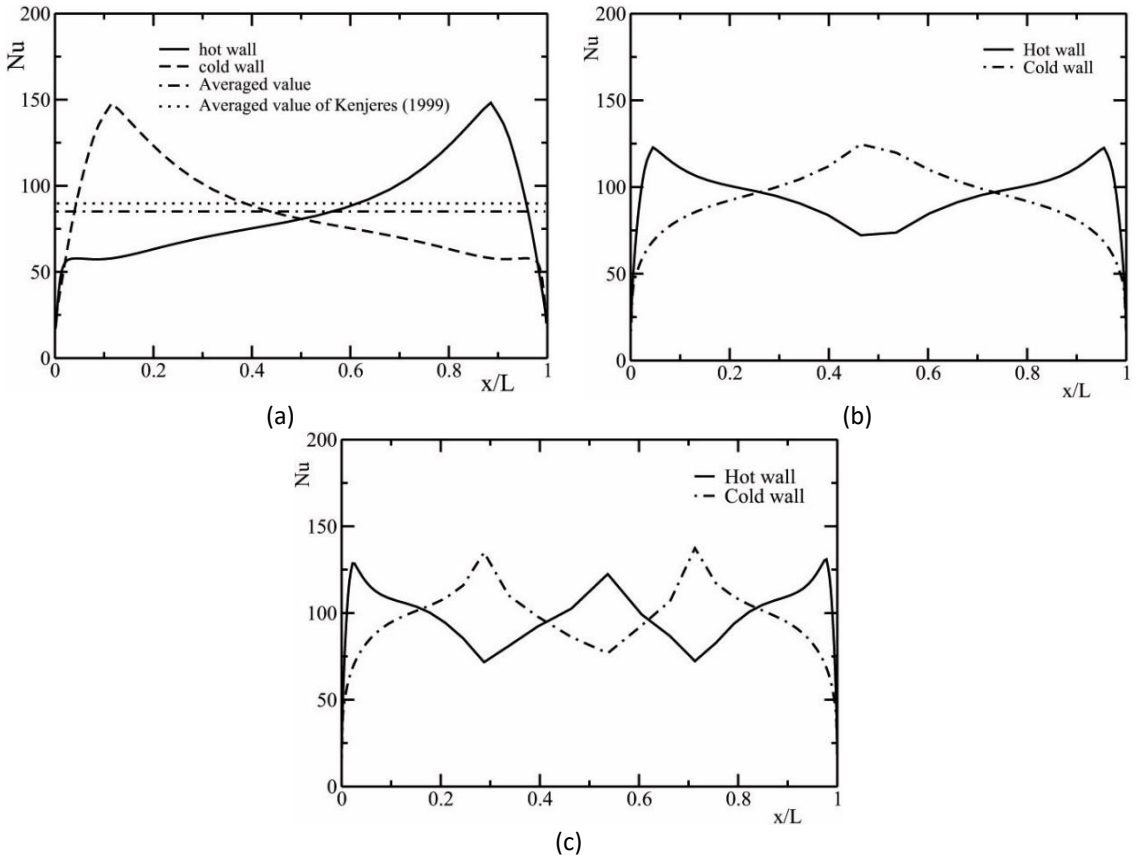

(a) (b)

(c)

Fig. 9. The plots of local Nusselt numbers along the walls for various height-to-length ratios (a) *H*/*L* = 1:1.5, (b) *H*/*L* = 1:4, and (c) *H*/*L* = 1:8

Figure 9(a), Figure 9(b), and Figure 9(c) show the plot of the local Nusselt number of hot and cold walls *H*/*L* = 1: 1.5, 1: 4, and 1: 8, respectively. The averaged local Nusselt numbers when *H*/*L* = 1: 1.5, 1: 4, and 1: 8 are 75, 95, and 105, respectively. It is clear from the figures that the total Nusselt number along the cavity in the hot and cold walls always produces a constant number.

4. Conclusions

The turbulence model of buoyancy extended eddy-viscosity with elliptic relaxation and algebraic approach has been applied to compute the Rayleigh-Benard convection for various height-to-length ratios. The model has been tested by numerical data from the horizontal channel and available experimental data. The model was able to reproduce very well the main features of heat and mass transfer in both the intensive turbulence region and the central cavity. The computed result also presents important insight of the structure of Rayleigh-Benard convection in various aspect ratio in cavity. A reasonable agreement was observed between the model and the direct numerical simulation. Similarly, the model also yields a nearly identical figure with the experimental data. In addition, the model has demonstrated reasonable improvement compared to previous models in the literature. It can be concluded that the model is relatively accurate and is able to capture and reveal realistic features of Rayleigh-Benard convection in cavity.

References

[1] Gunarjo, S. B. "Contribution to advanced modelling of turbulent natural and mixed convection." *PhD diss., Delft University of Technology* (2003).
[2] Clifford, Corey E., and Mark L. Kimber. "Assessment of RANS and LES turbulence models for natural convection in a differentially heated square cavity." *Numerical Heat Transfer, Part A: Applications* 78, no. 10 (2020): 560-594. https://doi.org/10.1080/10407782.2020.1803592
[3] Ji, Yingchun. "CFD modelling of natural convection in air cavities." *CFD Letters* 6, no. 1 (2014): 15-31.
[4] Saury, Didier, Abdelmadjid Benkhelifa, and François Penot. "Experimental determination of first bifurcations to unsteady natural convection in a differentially-heated cavity tilted from 0° to 180°." *Experimental Thermal and Fluid Science* 38 (2012): 74-84. https://doi.org/10.1016/j.expthermflusci.2011.11.009
[5] Demou, Andreas D., and Dimokratis GE Grigoriadis. "Direct numerical simulations of Rayleigh-Bénard convection in water with non-Oberbeck-Boussinesq effects." *Journal of Fluid Mechanics* 881 (2019): 1073-1096. https://doi.org/10.1017/jfm.2019.787
[6] Kenjereš, S., and K. Hanjalić. "Transient analysis of Rayleigh-Bénard convection with a RANS model." *International Journal of Heat and Fluid Flow* 20, no. 3 (1999): 329-340. https://doi.org/10.1016/S0142-727X(99)00007-7
[7] Clifford, Corey E., and Mark L. Kimber. "Assessment of RANS and LES turbulence models for natural convection in a differentially heated square cavity." *Numerical Heat Transfer, Part A: Applications* 78, no. 10 (2020): 560-594. https://doi.org/10.1080/10407782.2020.1803592
[8] van der Poel, Erwin P., Richard J. A. M. Stevens, Kazuyasu Sugiyama, and Detlef Lohse. "Flow states in two-dimensional Rayleigh-Bénard convection as a function of aspect-ratio and Rayleigh number." *Physics of Fluids* 24, no. 8 (2012). https://doi.org/10.1063/1.4744988
[9] Zhu, Xiaojue, Varghese Mathai, Richard J. A. M. Stevens, Roberto Verzicco, and Detlef Lohse. "Transition to the ultimate regime in two-dimensional Rayleigh-Bénard convection." *Physical Review Letters* 120, no. 14 (2018): 144502. https://doi.org/10.1103/PhysRevLett.120.144502
[10] Kenjereš, Sasa, S. B. Gunarjo, and K. Hanjalić. "Contribution to elliptic relaxation modelling of turbulent natural and mixed convection." *International Journal of Heat and Fluid Flow* 26, no. 4 (2005): 569-586. https://doi.org/10.1016/j.ijheatfluidflow.2005.03.007
[11] Kenjereš, Sasa. "Numerical modelling of complex buoyancy-driven flows." *PhD diss., Delft University of Technology* (1998).
[12] Ferziger, Joel H., and Milovan Perić. *Computational methods for fluid dynamics*. Springer, 2002. https://doi.org/10.1007/978-3-642-56026-2
[13] Patankar, Suhas. *Numerical heat transfer and fluid flow*. CRC Press, 2018. https://doi.org/10.1201/9781482234213
[14] Jones, W. Peter, and Brian Edward Launder. "The prediction of laminarization with a two-equation model of turbulence." *International Journal of Heat and Mass Transfer* 15, no. 2 (1972): 301-314. https://doi.org/10.1016/0017-9310(72)90076-2
[15] Wörner, Martin. "Direkte Simulation turbulenter Rayleigh-Bénard-Konvektion in flüssigem Natrium." *Kernforschungszentrum Karlsruhe* (1994).
[16] Dol, H. S., K. Hanjalić, and S. Kenjereš. "A comparative assessment of the second-moment differential and algebraic models in turbulent natural convection." *International Journal of Heat and Fluid Flow* 18, no. 1 (1997): 4-14. https://doi.org/10.1016/S0142-727X(96)00149-X

[17] Craft, T. J. *Second-moment modelling of turbulent scalar transport*. The University of Manchester (United Kingdom), 1991.
[18] Chu, T. Y., and R. J. Goldstein. "Turbulent convection in a horizontal layer of water." *Journal of Fluid Mechanics* 60, no. 1 (1973): 141-159. https://doi.org/10.1017/S0022112073000091